J. Fluid Mech. (2014), *vol.* 753, *pp.* 49–79. © Cambridge University Press 2014
doi:10.1017/jfm.2014.350

Electrophoresis of bubbles

Ory Schnitzer[1], Itzchak Frankel[2] and Ehud Yariv[1,†]

[1]Department of Mathematics, Technion – Israel Institute of Technology, Haifa 32000, Israel

[2]Department of Aerospace Engineering, Technion – Israel Institute of Technology, Haifa 32000, Israel

(Received 25 July 2013; revised 8 May 2014; accepted 17 June 2014;
first published online 16 July 2014)

Smoluchowski's celebrated electrophoresis formula is inapplicable to field-driven motion of drops and bubbles with mobile interfaces. We here analyse bubble electrophoresis in the thin-double-layer limit. To this end, we employ a systematic asymptotic procedure starting from the standard electrokinetic equations and a simple physicochemical interface model. This furnishes a coarse-grained macroscale description where the Debye-layer physics is embodied in effective boundary conditions. These conditions, in turn, represent a non-conventional driving mechanism for electrokinetic flows, where bulk concentration polarization, engendered by the interaction of the electric field and the Debye layer, results in a Marangoni-like shear stress. Remarkably, the electro-osmotic velocity jump at the macroscale level does not affect the electrophoretic velocity. Regular approximations are obtained in the respective cases of small zeta potentials, small ions, and weak applied fields. The nonlinear small-zeta-potential approximation rationalizes the paradoxical zero mobility predicted by the linearized scheme of Booth (*J. Chem. Phys.*, vol. 19, 1951, pp. 1331–1336). For large (millimetre-size) bubbles the pertinent limit is actually that of strong fields. We have carried out a matched-asymptotic-expansion analysis of this singular limit, where salt polarization is confined to a narrow diffusive layer. This analysis establishes that the bubble velocity scales as the 2/3-power of the applied-field magnitude and yields its explicit functional dependence upon a specific combination of the zeta potential and the ionic drag coefficient. The latter is provided to within an $O(1)$ numerical pre-factor which, in turn, is calculated via the solution of a universal (parameter-free) nonlinear flow problem. It is demonstrated that, with increasing field magnitude, all numerical solutions of the macroscale model indeed collapse on the analytic approximation thus obtained. Existing measurements of clean-bubble electrophoresis agree neither with present theory nor with previous models; we discuss this ongoing discrepancy.

Key words: drops and bubbles, electrohydrodynamic effects

1. Introduction

Electrokinetic phenomena are traditionally associated with the electrical double layer at solid–liquid interfaces. When a dielectric solid is brought into contact with an electrolyte solution it spontaneously acquires an immobile surface charge.

† Email address for correspondence: udi@technion.ac.il

https://doi.org/10.1017/jfm.2014.350 Published online by Cambridge University Press

Electrostatic attraction balanced by diffusion results in the formation of a diffuse ('Debye') layer, where counter-ions are in excess and co-ions in deficit relative to the electroneutral bulk. Charge relaxation towards the latter is characterized by the Debye screening thickness $1/\kappa^*$; the voltage drop ζ^* across this layer is known as the zeta potential.

A fundamental electrokinetic problem is that of electrophoresis, namely the motion of a colloidal particle (say of linear dimension a^*), suspended in an electrolyte solution (dielectric permittivity ϵ^*, shear viscosity μ^*), resulting from the application of a uniform electric field (say of magnitude E^*). This motion is governed by a highly nonlinear transport problem (Saville 1977) coupling ionic transport, electrostatics, and fluid flow. While this problem is generally intractable, a simple approximation is obtainable in the important limit

$$\kappa^* a^* \gg 1 \tag{1.1}$$

of thin double layers, commonly encountered in practice. Thus, Smoluchowski put forward his celebrated formula (Hunter 2000)

$$\mathscr{U}^* = \frac{\epsilon^* \zeta^*}{\mu^*} E^* \tag{1.2}$$

for the particle velocity $\mathscr{U}^*$. Smoluchowski's formula (1.2) was originally derived for a spherical particle of radius a^* (from which $\mathscr{U}^*$ is remarkably independent); it actually holds for particles of arbitrary shape (Morrison 1970). Smoluchowski's formula constitutes a *de facto* standard reference in colloid science. Thus, zeta-potential values inferred from (1.2) are commonly employed in correlating experimentally-observed trends and in estimating surface-charge densities.

The electrokinetic mechanism underlying solid–particle electrophoresis in the thin-double-layer limit is quite intuitive. All over the particle surface, Coulomb body forces give rise to a steep velocity profile on the Debye scale, appearing as an effective velocity slip on the macro (particle) scale; the electro-osmotic slip magnitude is proportional to the local value of the tangential electric field. Smoluchowski's formula (1.2) represents the response of a freely suspended force-free particle to the resulting slip-velocity distribution along the boundary. Its applicability is limited to neither weak fields (see Schnitzer & Yariv 2012*a*) nor small zeta potentials (although it breaks down at moderately large zeta potentials due to emergence of an effective surface-conduction mechanism, see O'Brien 1983).

It is well known that drops and bubbles also become charged when suspended in an electrolyte solution (Davis, James & Leckie 1978). In this context, the first documentation of electrophoretic migration was reported by Quincke (1861), who observed the motion of air bubbles in water. Electrophoretic motion of drops and bubbles is commonly used to estimate their interfacial charge density (McTaggart 1914; Yang *et al.* 2001); such estimates are important because this charge plays a key role in numerous colloidal phenomena (Russel, Saville & Schowalter 1989). Moreover, electrokinetic manipulation of drops and bubbles is frequently employed in microfluidic applications (Chang & Yeo 2010) and various lab-on-a-chip protocols (Huebner *et al.* 2008; Teh *et al.* 2008) such as sample injection (Liu & Dasgupta 1997) and drop microextraction (Choi *et al.* 2008).

As for a solid particle, the presence of charge on the interface of a fluid globule is accompanied by a diffuse Debye layer, where field-driven electro-osmosis is manifested as a local slip. This slip distribution, however, applies

https://doi.org/10.1017/jfm.2014.350 Published online by Cambridge University Press

here relative to a mobile boundary and hence does not by itself determine the velocity field in the electrolyte. Thus, there is no reason to expect Smoluchowski's formula to apply to such fluid globules. In fact, while the linear field dependence embodied in Smoluchowski's formula was both experientially observed (Kumar *et al.* 2006) and theoretically established (Schnitzer & Yariv 2012*b*) for solid particles, experimental measurements of bubble electrophoresis clearly indicate a field-dependent electrophoretic mobility (Kelsall *et al.* 1996*a*,*b*).

To date, there is no comparable thin-double-layer model of electrophoresis of drops and bubbles. Key investigations in the field have resorted to other approximations, essentially entailing two types of linearization schemes. The first, by Booth (1951), assumes zeta potentials which are small compared with the thermal voltage ($\approx$25 mV at room temperature, see (2.1) below); the second, by Baygents & Saville (1991), follows O'Brien & White (1978) by considering weak applied fields. Each of these approximations suffers from a serious shortcoming. Even when considering small zeta potentials (which does not seem to be the norm, see Graciaa *et al.* 1995), it is well known that a mere linearization often results in the overlooking of important phenomena associated with the intrinsic nonlinearity of the double-layer structure (Chang & Yeo 2010; Schnitzer, Frankel & Yariv 2013); indeed, when reduced to the thin-double-layer limit, the mobility expression derived by Booth (1951) for a gas bubble vanishes, which is incompatible with experimental observations. The shortcoming of the Baygents & Saville scheme has to do with the validity of the implicit assumption underlying the weak-field approximation, namely that a^*E^*, the potential drop associated with the applied field, is small compared with the thermal voltage (see §1.1 in Schnitzer *et al.* 2013). Even for micron-size drops this assumption is rather strained (Harper 2010), let alone for millimetric sizes. The importance of the above schemes notwithstanding, their limitations emphasize the desirability of a thin-double-layer approximation valid at arbitrary values (i.e. comparable to the thermal voltage) of both the zeta potential and a^*E^*. It is the goal of our contribution to develop such an approximation, on a par with the well-established theories existing for electrophoresis of solid particles.

The absence thus far of such approximate theory for electrophoresis of fluid globules may be attributed to the subtlety of the thin-double-layer limit in the context of mobile interfaces. Recall that any generic analysis of the flow about an interface separating two fluids involves the continuity there of both tangential velocity and shear stress. In a thin-double-layer electrophoresis problem, these boundary conditions apply at the microscale level. Clearly, velocity continuity does not carry over to the macroscale level; rather, the electro-osmotic Debye-layer profile transforms it into an effective slip condition. What is the macroscale counterpart of shear-stress condition? Answering this requires a systematic asymptotic analysis, of the type recently used by Schnitzer & Yariv (2012*a*) to highlight the thin-double-layer limit in the (more intuitive) context of solid surfaces.

As it turns out, the derivation of a self-contained leading-order macroscale description requires calculation of higher asymptotic orders when considering fluid interfaces. This difficulty suggests focusing on specific physicochemical scenarios which highlight the rich features of nonlinear free-surface electrokinetics. In a recent contribution (Schnitzer *et al.* 2013) we have addressed the limiting case of a highly conducting drop, which has been analysed in detail for weak fields by Ohshima, Healy & White (1984). We here consider another limiting case, which in a sense is the opposite extreme: an insulating gas bubble. Here charge transport is confined to the suspending liquid and the effect of internal circulation on the electrophoretic

https://doi.org/10.1017/jfm.2014.350 Published online by Cambridge University Press

motion is negligible. (This limit is more representative than that of a highly-conducing drop, where the shear-stress balance brings about a unique velocity amplification, see Ohshima *et al.* 1984.)

We employ the simplest physicochemical model of interfacial transport (Booth 1951). Thus, sorption of the salt ions is neglected, the surface-charge density is assumed uniform and fixed (e.g. due to the preferential adsorption of OH^- ions), and the interface is assumed clean of any surface-active agents capable of modifying the surface tension. To facilitate an uncluttered analysis we neglect the dielectric constant of the gas phase relative to that of the liquid; the latter is assumed a symmetric binary electrolyte, with the cationic and anionic diffusivities taken to be identical (as is approximately the case in KCl). To further simplify and focus the analysis we ignore the effect of gravity. The methodology employed in this paper would also be applicable to more sophisticated models where these assumptions are relaxed; see § 11.

As in our recent analysis of thin-double-layer transport about solid surfaces (Schnitzer & Yariv 2012*a*), we employ the differential equations of the standard electrokinetic model (Saville 1977). Supplemented by boundary conditions which represent the idealized interfaces considered by Booth (1951), as described above, these constitute a microscale model that serves as our starting point. A significant part of the present paper is devoted to 'coarse-graining' this model in the thin-double-layer limit, where the fluid domain is conceptually decomposed into a thin Debye layer in quasi-equilibrium, surrounding the interface, and the electroneutral bulk. Asymptotic matching between these two regions results in the requisite macroscale description, where the Debye-layer physics is represented by effective boundary conditions. In this description, the presumed uniform surface-charge density is manifested in a Debye-layer voltage ('zeta potential') which is uniform over the surface. As in the microscale model, this description is limited to neither weak fields nor small zeta potentials; compared with existing linearization schemes, this generality is a distinct advantage of the present approximation scheme.

The resulting macroscale description involves a mutual coupling between the leading-order flow and the (asymptotically small) salt-concentration perturbation. Because the latter is affected by the former through advection, the description is inherently nonlinear. Three parameters appear in the macroscale problem: the bubble zeta potential, the ion-drag coefficient, and the applied-field magnitude, the latter constituting the key 'input' to the problem. In principle, solving this problem yields the bubble velocity (the 'output'). With the effective removal of the scale disparity from the macroscale description, numerical solutions are readily obtained for arbitrary values of these parameters using standard methods. These reveal a nonlinear dependence of the bubble velocity upon the applied field (i.e. a non-constant electrophoretic 'mobility') when going beyond weak fields. The numerical solutions are supplemented by regular approximations, readily obtainable whenever one of the governing parameters is small; while only one of these approximations represents a weak-field linearization, all three of them result in a field-independent mobility.

As already mentioned, bubble sizes encountered in applications can be rather large, up to millimetres. It follows that the most important limit is perhaps that of strong fields, where the potential drop associated with the applied field is large. In this singular limit, strong convection confines the salt polarization to a narrow boundary layer, where diffusive salt fluxes emanating from the Debye layers are convected away. The thickness of this diffusive layer scales inversely with the $1/3$ power of the applied-field magnitude; this corresponds to fluid velocities that scale as its $2/3$ power.

https://doi.org/10.1017/jfm.2014.350 Published online by Cambridge University Press

The confinement of salt variations to a narrow layer where the tangential velocity is approximately uniform enables an analytic treatment of the nonlinear coupling between the salt concentration and fluid motion. Thus, use of integral transforms allows for an implicit solution for the salt polarization within the layer, leading in turn to a closed problem governing the flow in the homogeneous outer region. A rescaling of the flow variables transforms that problem into a universal one, independent of the three governing parameters. The numerically evaluated bubble-velocity data, similarly rescaled, indeed collapse on the curve predicted by this universal problem.

To the best of our knowledge, the only attempt thus far to develop a thin-double-layer model of bubble electrophoresis was carried out by Harper (2010). As in Booth (1951), Harper (2010) focused upon small zeta potentials. His results however are incompatible with those of Booth (1951). In § 11 we discuss this disagreement, as well as other aspects of Harper's work.

Our paper is arranged as follows. In the next section we formulate the microscale problem governing bubble electrophoresis. In § 3 we consider the thin-double-layer limit, describing the decomposition of the liquid domain into an electroneutral bulk and the Debye layer. In § 4 we analyse the leading-order Debye-layer transport, demonstrating that the shear-stress condition is trivially satisfied at this order, which leaves the flow indeterminate. The shear-stress condition at the next asymptotic order is analysed in § 5. The corresponding macroscale condition, expressed in terms of the salt-concentration perturbation, is derived in § 6. The problem governing the latter is described in § 7. The macroscale model, involving mutual coupling between the liquid flow and the bulk-concentration polarization, is recapitulated in § 8. In § 9 we present regular approximations in the respective limits of low zeta potentials, small ions, and weak fields. The important limit of strong fields is analysed in § 10. In § 11 we make concluding comments and outline future directions.

2. Problem formulation

A bubble (radius a^*) is suspended in an unbounded electrolyte solution of dielectric permittivity ϵ^* and viscosity μ^*. The electrolyte is symmetric (ionic valencies $\pm\mathscr{Z}$); at large distance from the bubble both ionic species thus possess identical concentrations, say c^*. For simplicity, we assume identical ionic diffusivity of both species, say D^*. A uniform electric field of magnitude E^* is externally applied, resulting in bubble motion with velocity $\mathscr{U}^*$ relative to the otherwise quiescent electrolyte. The value of $\mathscr{U}^*$ represents the lumped effect of the applied field. The key question is: how does $\mathscr{U}^*$ depend upon E^*?

We employ a dimensionless formulation, normalizing length variables by a^*, ionic concentrations by c^*, and electric potentials by the thermal voltage

$$\varphi^* = \frac{k^*T^*}{\mathscr{Z}e^*}, \tag{2.1}$$

in which k^*T^* is the Boltzmann temperature and e^* the proton charge. Stresses are normalized by the Maxwell scale $M^* = \epsilon^*\varphi^{*2}/a^{*2}$, which when balanced against viscous stresses yields the corresponding scale $u^* = a^*M^*/\mu^*(=\epsilon^*\varphi^{*2}/\mu^*a^*)$ used to normalize velocities.

The analysis is carried out in a reference frame translating with the bubble, wherein the problem is steady. The pertinent fields in the liquid domain are the ionic concentrations $c^{\pm}$, electric potential φ, and fluid velocity $\boldsymbol{u}$. These are governed by the following differential equations of the standard electrokinetic model.

https://doi.org/10.1017/jfm.2014.350 Published online by Cambridge University Press

(*a*) Nernst–Planck ion-conservation equations:

$$\nabla \cdot \boldsymbol{j}^{\pm} + \alpha \boldsymbol{u} \cdot \nabla c^{\pm} = 0 \tag{2.2}$$

wherein the ionic fluxes (normalized by $D^* c^*/a^*$)

$$\boldsymbol{j}^{\pm} = -\nabla c^{\pm} \mp c^{\pm} \nabla \varphi \tag{2.3}$$

represent the combined action of Brownian diffusion and electro-migration. The ionic-drag coefficient

$$\alpha = \frac{\epsilon^* \varphi^{*2}}{\mu^* D^*} \tag{2.4}$$

is independent of both bubble size a^* and ambient salt concentration c^*. Moreover, by the Stokes–Einstein relation, it is also independent of the liquid viscosity (Yariv, Schnitzer & Frankel 2011): as $\mu^* D^*$ is of the order $k^* T^*/d^*$, with d^* being the typical ionic size, α is of the order

$$\frac{\epsilon^* \varphi^{*2} d^*}{k^* T^*}. \tag{2.5}$$

For typical ions in aqueous solutions at room temperature, $\alpha \lesssim 0.5$ (Saville 1977). It is therefore considered here an $O(1)$ quantity.

(*b*) Poisson's equation:

$$-2\delta^2 \nabla^2 \varphi = c^+ - c^-. \tag{2.6}$$

Here

$$\delta = \frac{1}{\kappa^* a^*} \tag{2.7}$$

with the Debye width $1/\kappa^*$ defined by $\kappa^{*2} = 2\mathscr{Z} e^* c^*/\epsilon^* \varphi^*$.

(*c*) The continuity equation:

$$\nabla \cdot \boldsymbol{u} = 0 \tag{2.8}$$

(already tacitly used in (2.2)).

(*d*) Stokes's equation:

$$\nabla p = \nabla^2 \boldsymbol{u} + \nabla^2 \varphi \nabla \varphi, \tag{2.9}$$

accounting for Coulomb body forces. This equation expresses the divergence-free stress in the liquid,

$$\nabla \cdot (\boldsymbol{N} + \boldsymbol{M}) = 0, \tag{2.10}$$

wherein $\boldsymbol{N}$ is the Newtonian stress

$$\boldsymbol{N} = -p\boldsymbol{I} + \nabla \boldsymbol{u} + (\nabla \boldsymbol{u})^{\dagger} \tag{2.11}$$

(in which $\boldsymbol{I}$ is the idemfactor and † denotes transposition), and $\boldsymbol{M}$ is the Maxwell stress

$$\boldsymbol{M} = \nabla \varphi \nabla \varphi - \tfrac{1}{2} \nabla \varphi \cdot \nabla \varphi \, \boldsymbol{I}. \tag{2.12}$$

As is the standard practice for incompressible fluids, the isotropic term in the Maxwell stress associated with the density dependence of the dielectric constant is absorbed in the pressure p, see Schnitzer *et al.* (2013). Thus, when multiplied by an appropriate unit normal, $\boldsymbol{N} + \boldsymbol{M}$ still provides the true traction.

https://doi.org/10.1017/jfm.2014.350 Published online by Cambridge University Press

In specifying the conditions at the interface, we employ the simplest model, as discussed in § 1. This model consists of four key assumptions: (i) the surface tension is uniform, and is sufficiently strong to keep the bubble nearly spherical; (ii) the salt ions do not adsorb at the interface, nor do they cross it into the gas; (iii) the gas permittivity and viscosity are negligible relative to the corresponding values in the electrolyte, thus decoupling the gas phase from the hydrodynamic and electrostatic calculations; and (iv) the surface-charge density at the interface is uniform and is unaffected by the application of the field.

The boundary conditions are written using spherical polar coordinates (r, θ, ϖ), $r = 0$ at the bubble centre and $\theta = 0$ in the applied-field direction. Because of axial symmetry the vector fields $\boldsymbol{j}^{\pm}$ and $\boldsymbol{u}$ do not possess an azimuthal component; specifically, $\boldsymbol{u} = \hat{\boldsymbol{e}}_r u + \hat{\boldsymbol{e}}_\theta v$. Furthermore, all the pertinent fields are independent of the azimuthal angle ϖ.

Following assumption (i), the interfacial conditions apply at $r = 1$. They consist of:

(*a*) ionic no-flux

$$\hat{\boldsymbol{e}}_r \cdot \boldsymbol{j}^{\pm} = 0, \tag{2.13}$$

representing assumption (ii);

(*b*) flow impermeability

$$u = 0; \tag{2.14}$$

(*c*) Gauss's law

$$\frac{\partial \varphi}{\partial r} = -\delta^{-1}\sigma, \tag{2.15}$$

wherein $\sigma = \sigma^*/\epsilon^*\kappa^*\varphi^*$ is the dimensionless surface-charge density, and following assumption (iv), it is considered constant and uniform;

(*d*) vanishing shear stress

$$\frac{\partial v}{\partial r} - v = \delta^{-1}\sigma \frac{\partial \varphi}{\partial \theta}, \tag{2.16}$$

obtained by substituting (2.15) into (2.12). Note the absence from both (2.15) and (2.16) of contributions from the gas phase, following assumption (iii).

At large distances from the drop the ionic concentrations approach their reference value

$$c^{\pm} \to 1 \tag{2.17}$$

and the electric field becomes uniform

$$\nabla\varphi \to -\beta\hat{\boldsymbol{\imath}}. \tag{2.18}$$

Here

$$\beta = \frac{E^* a^*}{\varphi^*} \tag{2.19}$$

is the dimensionless magnitude of the applied field and $\hat{\boldsymbol{\imath}}$ a unit vector in its direction. In the co-moving frame the velocity field approaches a uniform stream

$$\boldsymbol{u} \to -\mathscr{U}\hat{\boldsymbol{\imath}} \tag{2.20}$$

in which $\mathscr{U} = \mathscr{U}^*/u^*$ is the bubble phoretic speed in the applied-field direction. This quantity is *a priori* unknown. Neglecting gravity effects, it is determined by

https://doi.org/10.1017/jfm.2014.350 Published online by Cambridge University Press

the requirement that the resultant force exerted on the bubble by the combination of Newtonian and Maxwell stresses (see (2.11) and (2.12)) vanishes:

$$\oint_{r=1} (\boldsymbol{N} + \boldsymbol{M}) \cdot \hat{\boldsymbol{e}}_r \, \mathrm{d}A = \boldsymbol{0}; \tag{2.21}$$

here, dA is a differential areal element, normalized by a^{*2}. In view of (2.10), the integral can be evaluated over any surface enclosing the bubble, with $\hat{\boldsymbol{n}}$, an outward-pointing unit vector normal to the surface, replacing $\hat{\boldsymbol{e}}_r$.

Subsequent analysis is facilitated by writing the preceding equations in terms of the mean ('salt') concentration (normalized by c^*) and volumetric charge density (normalized by $2\mathscr{Z}e^*c^*$)

$$c = \tfrac{1}{2}\left(c^+ + c^-\right), \quad q = \tfrac{1}{2}\left(c^+ - c^-\right), \tag{2.22a,b}$$

as well as the mean 'salt' flux (normalized by D^*c^*/a^*) and current density (normalized by $2\mathscr{Z}e^*D^*c^*/a^*$)

$$\boldsymbol{j} = \frac{\boldsymbol{j}^+ + \boldsymbol{j}^-}{2}, \quad \boldsymbol{i} = \frac{\boldsymbol{j}^+ - \boldsymbol{j}^-}{2}. \tag{2.23a,b}$$

The constitutive relations (2.3) then read

$$\boldsymbol{j} = -\boldsymbol{\nabla} c - q\boldsymbol{\nabla}\varphi, \quad \boldsymbol{i} = -\boldsymbol{\nabla} q - c\boldsymbol{\nabla}\varphi. \tag{2.24a,b}$$

Thus, mutual addition and subtraction of the ionic conservation equation (2.2) respectively yield the salt and charge balances

$$\boldsymbol{\nabla}\cdot\boldsymbol{j} + \alpha\boldsymbol{u}\cdot\boldsymbol{\nabla} c = 0, \quad \boldsymbol{\nabla}\cdot\boldsymbol{i} + \alpha\boldsymbol{u}\cdot\boldsymbol{\nabla} q = 0. \tag{2.25a,b}$$

In terms of the alternative variables, Poisson's equation (2.6) becomes

$$\delta^2\nabla^2\varphi = -q; \tag{2.26}$$

the no-flux conditions (2.13) read

$$\hat{\boldsymbol{e}}_r\cdot\boldsymbol{j} = 0, \quad \hat{\boldsymbol{e}}_r\cdot\boldsymbol{i} = 0; \tag{2.27a,b}$$

and the far-field conditions (2.17) become

$$c \to 1, \quad q \to 0. \tag{2.28a,b}$$

3. Thin-double-layer limit

The preceding coupled and highly nonlinear problem seems intractable. Moreover, in many realistic applications the Debye layer is extremely narrow compared with bubble size. This scale disparity gets in the way of numerical simulations by means of standard schemes.

It is however this very feature which allows analytic progress to be made. The corresponding thin-double-layer limit

$$\delta \ll 1 \tag{3.1}$$

https://doi.org/10.1017/jfm.2014.350 Published online by Cambridge University Press

is singular. This is evident from Poisson's equation (2.26) where the small parameter multiplies the highest derivative. Given this, it is natural to employ matched asymptotic expansions, where the liquid domain is conceptually decomposed into a narrow boundary layer (i.e. the Debye layer) in quasi-equilibrium, and the essentially electro-neutral bulk surrounding it. The $O(\delta)$-wide Debye layer is described using the stretched radial coordinate

$$Z = \frac{r-1}{\delta}. \tag{3.2}$$

The interface is accordingly given by $Z=0$. Hereafter, we regard r as a coarse-grained bulk-scale coordinate. Thus, $r=1$ represents the outer edge of the Debye layer, where asymptotic matching conceptually takes place. When taking the limit (3.1) we treat all remaining parameters as $O(1)$. In particular, the assumption $\sigma = O(1)$ implies negligible Dukhin numbers (see Schnitzer & Yariv 2012*a*).

In the bulk we employ asymptotic expansions of the generic form

$$f = f_0 + \delta f_1 + \cdots . \tag{3.3}$$

Equation (2.26) thus yields electro-neutrality at both $O(1)$ and $O(\delta)$

$$q_0 \equiv 0, \quad q_1 \equiv 0, \tag{3.4a,b}$$

implying that

$$c_0^{\pm} = c_0, \quad c_1^{\pm} = c_1. \tag{3.5a,b}$$

In view of (3.5*a*), the $O(1)$ salt flux and current density adopt the simplified forms

$$\boldsymbol{j}_0 = -\boldsymbol{\nabla} c_0, \quad \boldsymbol{i}_0 = -c_0 \boldsymbol{\nabla}\varphi_0. \tag{3.6a,b}$$

At leading-order, the salt and charge balances (2.25) then read

$$\nabla^2 c_0 = \alpha \boldsymbol{u}_0 \cdot \boldsymbol{\nabla} c_0, \quad \boldsymbol{\nabla}\cdot(c_0\boldsymbol{\nabla}\varphi_0) = 0, \tag{3.7a,b}$$

while the flow equations (2.8) and (2.9) retain their form

$$\boldsymbol{\nabla}\cdot\boldsymbol{u}_0 = 0, \quad \boldsymbol{\nabla} p_0 = \nabla^2 \boldsymbol{u}_0 + \nabla^2\varphi_0 \boldsymbol{\nabla}\varphi_0. \tag{3.8a,b}$$

The need to match with the bulk fields suggests the following expansions within the Debye layer:

$$c^{\pm} = C_0^{\pm}(Z,\theta) + \delta C_1^{\pm}(Z,\theta) + \cdots , \tag{3.9}$$

corresponding to $O(1)$ concentrations. Equivalently,

$$c = C_0(Z,\theta) + \delta C_1(Z,\theta) + \cdots , \quad q = Q_0(Z,\theta) + \delta Q_1(Z,\theta) + \cdots . \tag{3.10a,b}$$

We also postulate $O(1)$ electric potential

$$\varphi = \Phi_0(Z,\theta) + \delta\Phi_1(Z,\theta) + \cdots \tag{3.11}$$

and tangential speeds

$$v = V_0(Z,\theta) + \delta V_1(Z,\theta) + \cdots . \tag{3.12}$$

https://doi.org/10.1017/jfm.2014.350 Published online by Cambridge University Press

Leading-order matching with the bulk thus implies

$$C_0^{\pm} \to c_0, \quad \Phi_0 \to \varphi_0, \quad V_0 \to v_0 \quad \text{as } Z \to \infty. \tag{3.13a–c}$$

Hereafter, bulk-scale variables appearing in equations governing the Debye-layer fields are understood to be evaluated at the 'effective' boundary $r = 1$, and are accordingly considered functions of θ alone.

In view of the postulated $O(1)$ tangential speeds, the continuity equation (2.8) in conjunction with the impermeability condition (2.14) implies $O(\delta)$ radial speeds

$$u = \delta U_1(Z, \theta) + \cdots, \tag{3.14}$$

while from the leading $O(\delta^{-3})$ radial-momentum balance (see (2.9)) we find an $O(\delta^{-2})$ pressure

$$p = \delta^{-2} P_{-2}(Z, \theta) + \delta^{-1} P_{-1}(Z, \theta) + \cdots. \tag{3.15}$$

Matching with the $O(1)$ bulk pressure then requires that

$$P_{-2}, P_{-1} \to 0 \quad \text{as } Z \to \infty. \tag{3.16}$$

For similar reasons, the following derivatives must also vanish at large Z:

$$\frac{\partial \Phi_0}{\partial Z}, \frac{\partial V_0}{\partial Z} \to 0 \quad \text{as } Z \to \infty. \tag{3.17}$$

The requirement of asymptotic matching also suggests that the radial ionic fluxes are at most $O(1)$:

$$\hat{\boldsymbol{e}}_r \cdot \boldsymbol{j}^{\pm} = J_0^{\pm} + \delta J_1^{\pm} + \cdots; \tag{3.18}$$

in terms of the salt flux and current density, this implies the corresponding expansions

$$\hat{\boldsymbol{e}}_r \cdot \boldsymbol{j} = J_0 + \delta J_1 + \cdots, \quad \hat{\boldsymbol{e}}_r \cdot \boldsymbol{i} = I_0 + \delta I_1 + \cdots. \tag{3.19a,b}$$

4. Debye-layer leading-order analysis

4.1. *Gouy–Chapman structure*

The absence of $O(\delta^{-1})$ ionic fluxes in the postulated expansions (3.18) in conjunction with (2.3) yields leading-order Boltzmann distributions. Making use of the matching conditions (3.13) together with (3.5*a*) we then obtain

$$C_0^{\pm} = c_0 \mathrm{e}^{\mp \Psi} \tag{4.1}$$

wherein

$$\Psi = \Phi_0 - \varphi_0 \tag{4.2}$$

is the 'excess' Debye-layer potential. At $O(1)$, Poisson's equation (2.6) then reads

$$\frac{\partial^2 \Psi}{\partial Z^2} = c_0 \sinh \Psi. \tag{4.3}$$

A single integration in conjunction with (3.17) yields

$$\frac{\partial \Psi}{\partial Z} = -2\sqrt{c_0} \sinh \frac{\Psi}{2}. \tag{4.4}$$

https://doi.org/10.1017/jfm.2014.350 Published online by Cambridge University Press

In terms of Ψ, Gauss's condition (2.15) requires

$$\frac{\partial \Psi}{\partial Z} = -\sigma \quad \text{at } Z = 0, \tag{4.5}$$

while the matching condition (3.13*b*) becomes

$$\Psi \to 0 \quad \text{as } Z \to \infty. \tag{4.6}$$

Substitution of (4.4) thus yields

$$\sigma = 2\sqrt{c_0}\sinh\frac{\zeta}{2}, \tag{4.7}$$

relating σ to the 'zeta potential'

$$\zeta = \Psi(Z = 0), \tag{4.8}$$

namely the leading-order Debye-layer voltage.

Equation (4.4) in conjunction with (4.6) is readily integrated (Lyklema 1995) to provide the Gouy–Chapman distribution

$$\tanh\frac{\Psi}{4} = \mathrm{e}^{-Z\sqrt{c_0}}\tanh\frac{\zeta}{4}, \tag{4.9}$$

wherein (4.8) is used as a convenient alternative to the original boundary condition (4.5). The large-Z exponential decay of Ψ in conjunction with (4.1) implies that $C_0^{\pm}$ approach c_0 with a similar exponential rate. A 2–1 Van-Dyke matching (Van Dyke 1964) then requires that the corresponding $O(\delta)$ Debye-scale fields directly match their outer counterparts. In view of (3.5*b*), these conditions read

$$\Phi_1 \to \varphi_1, \quad C_1^{\pm} \to c_1 \quad \text{as } Z \to \infty. \tag{4.10a,b}$$

4.2. *Homogeneous bulk*

Consider now the $O(\delta^{-1})$ balances of the Nernst–Planck equations (2.2), affected by neither advection nor tangential fluxes:

$$\frac{\partial J_0^{\pm}}{\partial Z} = 0. \tag{4.11}$$

Use of the no-flux conditions (2.13) thus yields

$$J_0^{\pm} \equiv 0, \tag{4.12}$$

whereby J_0 and I_0 vanish as well. Asymptotic matching with the bulk counterparts (3.6) yields effective boundary conditions governing the bulk fields:

$$\frac{\partial c_0}{\partial r} = 0, \quad \frac{\partial \varphi_0}{\partial r} = 0 \quad \text{at } r = 1. \tag{4.13a,b}$$

It then follows from (3.7*a*) and (2.28*a*) that

$$c_0 \equiv 1. \tag{4.14}$$

This leading-order salt homogeneity has the following consequences.

https://doi.org/10.1017/jfm.2014.350 Published online by Cambridge University Press

(*a*) From (3.7*b*) we find that φ_0 is harmonic. Conditions (2.18) and (4.13*b*) thus yield the leading-order bulk potential as a combination of the applied field and a dipole:

$$\varphi_0 = -\beta\left(r + \frac{1}{2r^2}\right)\cos\theta. \tag{4.15}$$

(*b*) With φ_0 harmonic, (3.8*b*) degenerates to the homogenous Stokes equation

$$\boldsymbol{\nabla} p_0 = \nabla^2 \boldsymbol{u}_0. \tag{4.16}$$

(*c*) Upon applying the force-free condition at the outer edge of the Debye layer, equation (2.21) is now reinterpreted with $r=1$ representing the effective boundary. With the harmonic field φ_0 possessing the form (4.15), it is well known that the associated Maxwell stress integral vanishes (Rivette & Baygents 1996; Yariv 2006). At $O(1)$ we then obtain the condition of a vanishing hydrodynamic force,

$$\oint_{r=1} \boldsymbol{N}_0 \cdot \hat{\boldsymbol{e}}_r \,\mathrm{d}A = 0. \tag{4.17}$$

(*d*) Relation (4.7) reduces to

$$\sigma = 2\sinh\frac{\zeta}{2}. \tag{4.18}$$

The zeta potential is accordingly uniform, determined by (the presumably prescribed value of) σ. Hereafter, we employ ζ as a convenient parameter, considered known.

(*e*) With ζ being uniform, (4.9) implies that Ψ too is independent of θ and is accordingly a function of Z alone. The same is true of the leading-order salt concentration and charge density

$$C_0 = \cosh\Psi, \quad Q_0 = -\sinh\Psi, \tag{4.19a,b}$$

obtained from (4.1) and (4.14).

(*f*) With Ψ independent of θ, it follows from (4.2) that $\partial\Phi_0/\partial\theta$ is independent of Z, i.e. the $O(1)$ leading-order tangential electric field is uniform across the Debye layer.

Up until now, the Debye-layer structure is similar to that about a solid colloid (at zero Dukhin number), see Schnitzer & Yariv (2012*a*). Things change dramatically, however, once considering the resulting flow.

4.3. *Flow indeterminacy*

The leading $O(\delta^{-3})$ momentum balance in the radial direction reads (see (2.9))

$$\frac{\partial P_{-2}}{\partial Z} = \frac{\mathrm{d}^2\Psi}{\mathrm{d}Z^2}\frac{\mathrm{d}\Psi}{\mathrm{d}Z}. \tag{4.20}$$

Integration in conjunction with the decay conditions (3.16) and (3.17) yields

$$P_{-2} = \frac{1}{2}\left(\frac{\mathrm{d}\Psi}{\mathrm{d}Z}\right)^2. \tag{4.21}$$

https://doi.org/10.1017/jfm.2014.350 Published online by Cambridge University Press

Since P_{-2} turns out to be independent of θ, the leading $O(\delta^{-2})$ momentum balance in the θ direction reads (see (4.2))

$$0 = \frac{\partial^2 V_0}{\partial Z^2} + \frac{\mathrm{d}^2 \Psi}{\mathrm{d}Z^2}\frac{\partial \varphi_0}{\partial \theta}. \tag{4.22}$$

A single integration in conjunction with the large-Z condition (3.17) yields the $O(\delta^{-1})$ shear distribution

$$\frac{\partial V_0}{\partial Z} = -\frac{\mathrm{d}\Psi}{\mathrm{d}Z}\frac{\partial \varphi_0}{\partial \theta}. \tag{4.23}$$

An additional integration from Z to ∞, in conjunction with (4.6) and the matching requirement

$$V_0 \to v_0 \quad \text{as } Z \to \infty \tag{4.24}$$

yields the velocity profile

$$v_0 - V_0 = \Psi \frac{\partial \varphi_0}{\partial \theta}. \tag{4.25}$$

Evaluating at $Z = 0$ using (4.8) yields the velocity jump across the Debye layer

$$v_0 - V_0(Z = 0) = \zeta \frac{\partial \varphi_0}{\partial \theta}. \tag{4.26}$$

In the case of a solid particle of moderate zeta potential, where the preceding derivation applies as well (Schnitzer & Yariv 2012*a*), the no-slip condition determines $V_0(Z = 0)$; then, (4.26) provides an effective slip condition for v_0. Here, since the interface is mobile, V_0 at $Z = 0$ is *a priori* unknown. This velocity indeterminacy distinguishes electro-osmotic flows about fluid interfaces.

Consistently with the statement of the microscale problem, we wish to obtain an effective condition exclusively involving macroscale fields within the liquid. Such a condition is obtainable from the shear-stress balance (2.16). The leading $O(\delta^{-1})$ balance, in conjunction with (4.2), reads

$$\frac{\partial V_0}{\partial Z} = \sigma \frac{\partial \varphi_0}{\partial \theta} \quad \text{at } Z = 0. \tag{4.27}$$

Substitution of (4.23) in conjunction with (4.5) reveals, however, that (4.27) is trivially satisfied. To obtain the requisite condition we thus need to proceed to the $O(1)$ balance of the shear-stress condition (2.16),

$$\frac{\partial V_1}{\partial Z} - V_0 = \sigma \frac{\partial \Phi_1}{\partial \theta} \quad \text{at } Z = 0. \tag{4.28}$$

This, in turn, requires the analysis of the Debye layer to one higher asymptotic order.

5. $O(1)$ shear-stress condition

Using (2.9), the radial momentum equation at $O(\delta^{-2})$ reads

$$\frac{\partial P_{-1}}{\partial Z} = 2\left(\frac{\mathrm{d}\Psi}{\mathrm{d}Z}\right)^2 + \frac{\partial}{\partial Z}\left(\frac{\mathrm{d}\Psi}{\mathrm{d}Z}\frac{\partial \Phi_1}{\partial Z}\right), \tag{5.1}$$

https://doi.org/10.1017/jfm.2014.350 Published online by Cambridge University Press

where the first term on the right-hand side appears due to the interface curvature. Integrating from Z to ∞ using (3.16) and the large-Z exponential decay of Ψ (see (4.9)) we obtain

$$-P_{-1} = 8\int_Z^\infty \sinh^2\frac{\Psi(Z')}{2}\,\mathrm{d}Z' - \frac{\mathrm{d}\Psi}{\mathrm{d}Z}\frac{\partial\Phi_1}{\partial Z}. \tag{5.2}$$

Performing the integration using (4.4) yields

$$P_{-1} = -16\sinh^2\frac{\Psi}{4} + \frac{\mathrm{d}\Psi}{\mathrm{d}Z}\frac{\partial\Phi_1}{\partial Z}. \tag{5.3}$$

Substituting into the $O(\delta^{-1})$ momentum balance in the θ direction

$$\frac{\partial P_{-1}}{\partial\theta} = \frac{\partial^2 V_1}{\partial Z^2} + 2\frac{\partial V_0}{\partial Z} + \left(\frac{\partial^2\Phi_1}{\partial Z^2} + 2\frac{\mathrm{d}\Psi}{\mathrm{d}Z}\right)\frac{\partial\varphi_0}{\partial\theta} + \frac{\mathrm{d}^2\Psi}{\mathrm{d}Z^2}\frac{\partial\Phi_1}{\partial\theta} - Z\frac{\mathrm{d}^2\Psi}{\mathrm{d}Z^2}\frac{\partial\varphi_0}{\partial\theta} \tag{5.4}$$

while making use of (4.23) and the θ independence of Ψ, we obtain

$$\frac{\partial^2 V_1}{\partial Z^2} = \frac{\partial^2\Phi_1}{\partial Z\partial\theta}\frac{\mathrm{d}\Psi}{\mathrm{d}Z} - \frac{\partial^2\Phi_1}{\partial Z^2}\frac{\partial\varphi_0}{\partial\theta} - \frac{\mathrm{d}^2\Psi}{\mathrm{d}Z^2}\frac{\partial\Phi_1}{\partial\theta} + Z\frac{\mathrm{d}^2\Psi}{\mathrm{d}Z^2}\frac{\partial\varphi_0}{\partial\theta}. \tag{5.5}$$

Integrating over Z from 0 to ∞ using the $O(1)$ matching conditions

$$\frac{\partial V_1}{\partial Z} \to \frac{\partial v_0}{\partial r}, \quad \frac{\partial\Phi_1}{\partial Z} \to \frac{\partial\varphi_0}{\partial r} \quad \text{as } Z\to\infty \tag{5.6a,b}$$

together with the homogeneous Neumann conditions (4.13*b*) and (see (2.15))

$$\frac{\partial\Phi_1}{\partial Z} = 0 \quad \text{at } Z = 0 \tag{5.7}$$

yields

$$\frac{\partial V_1}{\partial Z}(Z=0) - \frac{\partial v_0}{\partial r} = \int_0^\infty\left(\frac{\mathrm{d}^2\Psi}{\mathrm{d}Z^2}\frac{\partial\Phi_1}{\partial\theta} - \frac{\mathrm{d}\Psi}{\mathrm{d}Z}\frac{\partial^2\Phi_1}{\partial Z\partial\theta} - Z\frac{\mathrm{d}^2\Psi}{\mathrm{d}Z^2}\frac{\partial\varphi_0}{\partial\theta}\right)\mathrm{d}Z. \tag{5.8}$$

Integrating by parts the first and third terms of the integrand using (4.5), (4.6) and (4.8) yields

$$\frac{\partial V_1}{\partial Z}(Z=0) = \frac{\partial v_0}{\partial r} + \sigma\frac{\partial\Phi_1}{\partial\theta} - \zeta\frac{\partial\varphi_0}{\partial\theta} - 2\int_0^\infty\frac{\mathrm{d}\Psi}{\mathrm{d}Z}\frac{\partial^2\Phi_1}{\partial Z\partial\theta}\,\mathrm{d}Z. \tag{5.9}$$

Substitution of both (4.26) and (5.9) into the shear-stress condition (4.28) eventually yields

$$\frac{\partial v_0}{\partial r} - v_0 = 2\int_0^\infty\frac{\mathrm{d}\Psi}{\mathrm{d}Z}\frac{\partial^2\Phi_1}{\partial Z\partial\theta}\,\mathrm{d}Z \quad \text{at } r = 1. \tag{5.10}$$

Upon evaluation of Φ_1, (5.10) provides the requisite effective condition at $r = 1$, describing a macroscale stress jump across the entire layer (the interface and surrounding Debye layer). Note that a second effective condition

$$u_0 = 0 \quad \text{at } r = 1, \tag{5.11}$$

simply follows from the Debye-layer scaling of the radial speeds, see (3.14).

https://doi.org/10.1017/jfm.2014.350 Published online by Cambridge University Press

6. Debye-layer analysis: the next asymptotic order

The potential Φ_1 is governed by the $O(\delta)$ balance of Poisson's equation (2.6), namely

$$\frac{\partial^2 \Phi_1}{\partial Z^2} + 2\frac{\mathrm{d}\Psi}{\mathrm{d}Z} = \frac{C_1^- - C_1^+}{2}. \tag{6.1}$$

To calculate $C_1^{\pm}$ we recall the zero $O(1)$ radial fluxes, see (4.12). Use of (2.3) yields the differential equations

$$\mp C_0^{\pm}\frac{\partial \Phi_1}{\partial Z} \mp C_1^{\pm}\frac{\partial \Phi_0}{\partial Z} - \frac{\partial C_1^{\pm}}{\partial Z} = 0. \tag{6.2}$$

Solving these in terms of Φ_1 we obtain, using the matching conditions (4.10),

$$C_1^{\pm} = (c_1 \pm \varphi_1 \mp \Phi_1)\mathrm{e}^{\mp\Psi}. \tag{6.3}$$

In view of the absence of convection at this order, the ionic concentrations at $O(\delta)$ are, too, Boltzmann distributed. Substituting into (6.1) yields

$$\left(\frac{\partial^2}{\partial Z^2} - \cosh\Psi\right)\Phi_1 = -2\frac{\mathrm{d}\Psi}{\mathrm{d}Z} + c_1\sinh\Psi - \varphi_1\cosh\Psi. \tag{6.4}$$

This equation is supplemented by (4.10*a*) and (5.7). In (5.10) we only need the derivative $\partial\Phi_1/\partial\theta$, which satisfies

$$\left(\frac{\partial^2}{\partial Z^2} - \cosh\Psi\right)\frac{\partial \Phi_1}{\partial \theta} = \frac{\partial c_1}{\partial \theta}\sinh\Psi - \frac{\partial \varphi_1}{\partial \theta}\cosh\Psi. \tag{6.5}$$

A particular integral of (6.5), satisfying the requisite large-Z approach to $\partial\varphi_1/\partial\theta$, is

$$-2\frac{\partial c_1}{\partial \theta}\frac{Z\mathrm{e}^{-Z}\tanh\dfrac{\zeta}{4}}{1-\mathrm{e}^{-2Z}\tanh^2\dfrac{\zeta}{4}} + \frac{\partial \varphi_1}{\partial \theta}. \tag{6.6}$$

One complementary solution of (6.5) which decays at large Z is

$$\frac{\mathrm{e}^{-Z}}{1-\mathrm{e}^{-2Z}\tanh^2\dfrac{\zeta}{4}}. \tag{6.7}$$

The other solution diverges at large Z and is therefore rejected. The coefficient multiplying (6.7) is readily determined by means of condition (5.7). Substitution of the resulting expression for $\partial\Phi_1/\partial\theta$ into (5.10) and evaluation of the integral on the right-hand side furnishes the effective shear-stress condition

$$\frac{\partial v_0}{\partial r} - v_0 = -4\frac{\sinh^2\dfrac{\zeta}{4}}{\cosh\dfrac{\zeta}{2}}\frac{\partial c_1}{\partial \theta} \quad \text{at } r = 1. \tag{6.8}$$

At this point, one might have expected an additional shear-stress term linear in the local electric field. Since the leading-order tangential field within the Debye

https://doi.org/10.1017/jfm.2014.350 Published online by Cambridge University Press

layer is transversely uniform (see item (*f*) at the conclusion of § 4.2), such a term would locally be proportional to the product of that field and the net $O(1)$ double-layer charge (per unit area) at any given location (θ and ϖ) on the drop surface. Applying Gauss's law to a slab-shaped control volume spanning the entire double layer (including the charged bubble surface) using (4.13*b*) and the presumably negligible electric displacement within the bubble, it is readily verified that this net charge vanishes.

7. Salt perturbation in the bulk

Condition (6.8) couples the leading-order bulk flow to the salt perturbation c_1. Use of (2.25*a*) and (4.14) reveals that c_1 is governed by the advection–diffusion equation

$$\nabla^2 c_1 = \alpha \boldsymbol{u}_0 \cdot \boldsymbol{\nabla} c_1, \tag{7.1}$$

while (2.28*a*) implies a far-field decay. The effective condition at $r = 1$ follows from asymptotic matching of the leading $O(\delta)$ radial salt flux (see (2.24*a*), (3.4) and (3.19*a*)):

$$\frac{\partial c_1}{\partial r}(r=1) = -J_1(Z \to \infty). \tag{7.2}$$

To calculate $J_1(Z \to \infty)$ we follow the standard procedure of integrating the Debye-scale salt balance across the Debye layer (cf. Hinch *et al.* 1984). At $O(1)$, this balance (see (2.24) and (2.25)) reads

$$\frac{\partial J_1}{\partial Z} + 3\beta \sinh\Psi \cos\theta + \alpha U_1 \frac{\mathrm{d}C_0}{\mathrm{d}Z} = 0, \tag{7.3}$$

where the second term represents the contribution of the non-uniform $O(1)$ tangential salt flux. This purely electro-migratory contribution (see (2.24*a*)) is calculated using (4.15), (4.19), and the θ-independence of Ψ. Integrating from 0 to ∞ we find, using the no-flux condition (2.27*a*),

$$J_1(Z \to \infty) = -3\beta \cos\theta \int_0^\infty \sinh\Psi \,\mathrm{d}Z - \alpha \int_0^\infty U_1 \frac{\mathrm{d}C_0}{\mathrm{d}Z}\,\mathrm{d}Z. \tag{7.4}$$

By the $O(1)$ Debye-scale continuity equation

$$\frac{\partial U_1}{\partial Z} = -\frac{1}{\sin\theta}\frac{\partial}{\partial\theta}(V_0 \sin\theta), \tag{7.5}$$

the last integral in (7.4) is obtained via integration by parts (upon replacing C_0 by $C_0 - 1$):

$$J_1(Z \to \infty) = -3\beta \cos\theta \int_0^\infty \sinh\Psi \,\mathrm{d}Z + \frac{\alpha}{\sin\theta}\frac{\mathrm{d}}{\mathrm{d}\theta}\left[\sin\theta \int_0^\infty (C_0 - 1) V_0 \,\mathrm{d}Z\right] \tag{7.6}$$

where the boundary term at $Z = 0$ vanishes by the impermeability condition (2.14) and that at $Z \to \infty$ vanishes due to the exponential decay of $C_0 - 1$, which dominates the

https://doi.org/10.1017/jfm.2014.350 Published online by Cambridge University Press

linear growth with Z of U_1 (evident from (4.25) and (7.5)). Substitution of (4.19) and (4.25), while making use of the integrals (obtained using (4.4))

$$\int_0^\infty \sinh\Psi\,\mathrm{d}Z = 2\sinh\frac{\zeta}{2}, \quad \int_0^\infty (\cosh\Psi - 1)\,\mathrm{d}Z = 4\sinh^2\frac{\zeta}{4}, \tag{7.7a,b}$$

$$\int_0^\infty \Psi(\cosh\Psi - 1)\,\mathrm{d}Z = 2\zeta\cosh\frac{\zeta}{2} - 4\sinh\frac{\zeta}{2}, \tag{7.8}$$

we find

$$J_1(Z\to\infty) = -6\beta(1+2\alpha)\sinh\frac{\zeta}{2}\cos\theta + 6\alpha\beta\zeta\cosh\frac{\zeta}{2}\cos\theta - \frac{4\alpha\sinh^2\dfrac{\zeta}{4}}{\sin\theta}\frac{\mathrm{d}}{\mathrm{d}\theta}(v_0\sin\theta)\,. \tag{7.9}$$

8. Macroscale problem

8.1. *Recapitulation*

We here recapitulate the macroscale model representing bulk-scale transport in the limit $\delta\to 0$. For brevity we omit indices. The electric potential and velocities thus correspond to the leading-order terms in the original expansion (3.3); the quantity c, however, now represents the salt-excess concentration (relative to the ambient value c^*) normalized by $c^*\delta$.

This concentration satisfies the the advection–diffusion equation

$$\nabla^2 c = \alpha\boldsymbol{u}\cdot\boldsymbol{\nabla}c, \tag{8.1}$$

the Neumann-type condition at $r=1$ (see (7.2) and (7.9))

$$\frac{\partial c}{\partial r} = 6\beta(1+2\alpha)\sinh\frac{\zeta}{2}\cos\theta - 6\alpha\beta\zeta\cosh\frac{\zeta}{2}\cos\theta + \frac{4\alpha\sinh^2\dfrac{\zeta}{4}}{\sin\theta}\frac{\partial}{\partial\theta}(v\sin\theta)\,, \tag{8.2}$$

wherein ζ is related to σ through (4.18), and the requirement of attenuation at infinity

$$c\to 0 \quad \text{as } r\to\infty. \tag{8.3}$$

The liquid velocity is governed by the continuity

$$\boldsymbol{\nabla}\cdot\boldsymbol{u} = 0 \tag{8.4}$$

and Stokes (see (4.14) *et seq.*)

$$\boldsymbol{\nabla}p = \nabla^2\boldsymbol{u} \tag{8.5}$$

equations, together with effective conditions at $r=1$, consisting of shear-stress jump (see (6.8))

$$\frac{\partial v}{\partial r} - v = -4\frac{\sinh^2\dfrac{\zeta}{4}}{\cosh\dfrac{\zeta}{2}}\frac{\partial c}{\partial\theta}, \tag{8.6}$$

and impermeability (see (5.11))

$$u = 0. \tag{8.7}$$

These are supplemented by the requirement of a far-field approach to a uniform streaming velocity

$$u\to -\mathscr{U}\cos\theta, \quad v\to\mathscr{U}\sin\theta \quad \text{as } r\to\infty. \tag{8.8a,b}$$

https://doi.org/10.1017/jfm.2014.350 Published online by Cambridge University Press

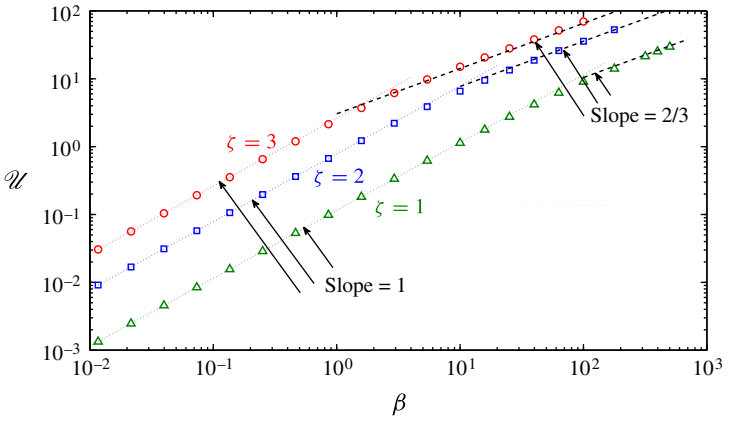


FIGURE 1. (Colour online) Variation of $\mathscr{U}$, the electrophoretic velocity, with β, the dimensionless field intensity, for $\alpha = 0.2$ and the indicated values of ζ, as obtained from a numerical solution of the macroscale problem (8.1)–(8.9). The dotted lines depict the respective weak-field approximations (9.19). The dashed lines mark the corresponding strong-field asymptotes, derived in § 10, which grow like $\beta^{2/3}$.

The electrophoretic velocity $\mathscr{U}$ appearing in the latter is, in turn, determined from the force-free condition (now involving only the Newtonian stress $\boldsymbol{N} = -p\boldsymbol{I} + \boldsymbol{\nabla u} + (\boldsymbol{\nabla u})^{\dagger}$, see (4.17))

$$\oint_{r=1} \boldsymbol{N} \cdot \hat{\boldsymbol{n}} \, \mathrm{d}A = \boldsymbol{0}. \tag{8.9}$$

With the governing Stokes equations, satisfaction of this condition is guaranteed by omitting the Stokeslet term in the velocity field (Batchelor 1967).

8.2. *Numerical solutions*

The preceding system of equations is coupled through both the advection term in (8.1) and the boundary conditions (8.2) and (8.6). The former also introduces an inherent nonlinearity, which appears to preclude a closed-form solution of this problem. Nonetheless, a numerical solution is readily obtained. The scheme consists of expanding the salt perturbation in terms of Legendre polynomials of $\cos\theta$ and representing the Stokes flow using the familiar eigenfunction expansion in spherical coordinates (Happel & Brenner 1965). This reduces the problem to an infinite system of (coupled and nonlinear) ordinary differential equations (ODEs) in r, which may be solved by a controlled truncation procedure. This procedure is essentially the same as that detailed by Khair (2013) in the context of a different physical problem.

We have applied this scheme for $\zeta = 1, 2, 3$ and the typical value $\alpha = 0.2$. Figure 1 depicts on a logarithmic scale the calculated electrophoretic velocity as a function of the field magnitude β. For all values of ζ presented and $\beta \lesssim O(1)$ we observe a linear variation of $\mathscr{U}$ with β (see § 9.3). At larger values of β a transition to a nonlinear power law takes place (see § 10).

9. Linearized solutions: low zeta potentials, small ions and weak fields

There are three different limits wherein the advection term in (8.1) is negligible, rendering the problem linear, with closed-form expressions readily derived for the

https://doi.org/10.1017/jfm.2014.350 Published online by Cambridge University Press

bubble velocity. These are the limits of weakly-charged bubbles ($\sigma \ll 1$), small ions ($\alpha \ll 1$), and weak applied fields ($\beta \ll 1$), respectively. Note that in the former two limits linearity persists even when the applied field is not restricted to be small.

9.1. *Weakly-charged bubbles*

Relation (4.18) gives

$$\zeta \ll 1. \tag{9.1}$$

The governing equations suggest an $O(\zeta)$ excess-salt concentration

$$c = \zeta \grave{c} + \cdots, \tag{9.2}$$

and an $O(\zeta^3)$ flow

$$\boldsymbol{u} = \zeta^3 \grave{\boldsymbol{u}} + \cdots, \quad \mathscr{U} = \zeta^3 \grave{\mathscr{U}} + \cdots. \tag{9.3a,b}$$

The salt perturbation $\grave{c}$ is governed by Laplace's equation, the Neumann condition

$$\frac{\partial \grave{c}}{\partial r} = 3\beta \cos\theta, \tag{9.4}$$

and decay at infinity. The solution is the dipole

$$\grave{c} = -\frac{3\beta}{2r^2} \cos\theta. \tag{9.5}$$

Both the shear-stress condition (8.6) and the far-field approach (8.8) suggest that $v \propto \sin\theta$. The possible Stokeslet-free flow solution satisfying (8.8) and the impermeability condition (8.7) is a combination of a uniform stream and a doublet

$$\grave{u} = \grave{\mathscr{U}} \left(1 - \frac{1}{r^3}\right) \cos\theta, \quad \grave{v} = \grave{\mathscr{U}} \left(1 + \frac{1}{2r^3}\right) \sin\theta. \tag{9.6a,b}$$

Condition (8.6) then yields the bubble speed

$$\grave{\mathscr{U}} = \frac{\beta}{8}. \tag{9.7}$$

The zero velocity predicted by Booth (1951) is simply a consequence of the restriction of his small-zeta-potential analysis to terms linear in ζ.

9.2. *Small ions*

For small ions (2.5) implies

$$\alpha \to 0, \tag{9.8}$$

whereby the advection term in (8.1) is again negligible. The excess-salt concentration is harmonic, satisfying the Neumann condition

$$\frac{\partial c}{\partial r} = 6\beta \sinh\frac{\zeta}{2} \cos\theta, \tag{9.9}$$

https://doi.org/10.1017/jfm.2014.350 Published online by Cambridge University Press

and far-field attenuation. The solution is the dipole

$$c = -\frac{3\beta \sinh\frac{\zeta}{2}}{r^2}\cos\theta. \tag{9.10}$$

The velocity field possesses the same form as (9.6),

$$u = \mathscr{U}\left(1-\frac{1}{r^3}\right)\cos\theta, \quad v = \mathscr{U}\left(1+\frac{1}{2r^3}\right)\sin\theta. \tag{9.11a,b}$$

Condition (8.6) thus yields

$$\mathscr{U} = 4\beta \tanh\frac{\zeta}{2}\sinh^2\frac{\zeta}{4}. \tag{9.12}$$

Note that for small zeta potentials

$$\mathscr{U} \sim \frac{\beta\zeta^3}{8} \tag{9.13}$$

in agreement with (9.3) and (9.7).

9.3. *Weak fields*

For weak applied fields,

$$\beta \ll 1, \tag{9.14}$$

we employ the linearization

$$c = \beta\grave{c} + \cdots, \quad \boldsymbol{u} = \beta\grave{\boldsymbol{u}} + \cdots, \quad \mathscr{U} = \beta\grave{\mathscr{U}} + \cdots, \tag{9.15a–c}$$

with a similar expansion for p. The corresponding salt perturbation $\grave{c}$ is governed by Laplace's equation, the Neumann condition

$$\frac{\partial\grave{c}}{\partial r} = 6(1+2\alpha)\sinh\frac{\zeta}{2}\cos\theta - 6\alpha\zeta\cosh\frac{\zeta}{2}\cos\theta + 4\alpha\sinh^2\frac{\zeta}{4}\frac{1}{\sin\theta}\frac{\partial}{\partial\theta}\left(\grave{v}\sin\theta\right), \tag{9.16}$$

and decay at infinity. The fluid velocity $\grave{\boldsymbol{u}}$ is governed by the Stokes equations, the shear-jump condition

$$\frac{\partial\grave{v}}{\partial r} - \grave{v} = -4\frac{\sinh^2\frac{\zeta}{4}}{\cosh\frac{\zeta}{2}}\frac{\partial\grave{c}}{\partial\theta}, \tag{9.17}$$

impermeability at $r=1$, and the far-field approach to a uniform stream

$$\grave{u} \to -\grave{\mathscr{U}}\cos\theta, \quad \grave{v} \to \grave{\mathscr{U}}\sin\theta \quad \text{as } r\to\infty. \tag{9.18a,b}$$

Unlike the preceding limits, the salt perturbation and flow are here mutually coupled. Technically, the solution is straightforward. The salt perturbation is a dipole, say $D\cos\theta/r^2$, while the flow possesses the form (9.6). Conditions (9.16) and (9.17)

https://doi.org/10.1017/jfm.2014.350 Published online by Cambridge University Press

provide a pair of linear algebraic equations governing D and $\grave{\mathscr{U}}$, whose solution yields

$$\grave{\mathscr{U}} = \frac{4(1+2\alpha)\sinh\frac{\zeta}{2}\sinh^2\frac{\zeta}{4} - 4\alpha\zeta\cosh\frac{\zeta}{2}\sinh^2\frac{\zeta}{4}}{\cosh\frac{\zeta}{2} - 8\alpha\sinh^4\frac{\zeta}{4}}. \tag{9.19}$$

Note that for small ζ we recover (9.13). The mutual coupling in the boundary conditions results here in an apparent singularity for $\alpha = \cosh(\zeta/2)/8\sinh^4(\zeta/4)$. The appearance of this finite-α singularity may be attributed to a bifurcation of the nonlinear problem which for $\beta = 0$ occurs at this specific value. For all finite values of β the nonlinear convection term neglected here in the course of linearization regularizes the solution.

The agreement of the weak-field approximation (9.19) with the numerical solutions of the nonlinear macroscale problem is evident in figure 1 for $\beta \lesssim O(1)$.

10. Strong fields

We now turn to consider the strong-field limit

$$\beta \gg 1 \tag{10.1}$$

which, in view of the relatively large size of bubbles is the one pertinent in many applications (see (2.19)). For the 80 μm bubbles in the experiments of Kelsall *et al.* (1996*b*), for example, $\beta \approx 20$ under the strongest electric field applied (Harper 2010). Evidently, β will be much larger for millimetric bubbles.

10.1. *Scaling arguments: diffusive boundary layer*

Under a strong electric field we expect the bubble velocity $\mathscr{U}$ to be asymptotically large. Since the electric field affects the macroscale flow only through the distribution of c at $r = 1$ (see (8.6)), this implies a large concentration deviation, whose scaling $\lambda(\beta)$ remains to be determined. Thus, we postulate

$$c = O(\lambda) \quad \text{for } \beta \gg 1 \tag{10.2}$$

where

$$\lambda(\beta) \gg 1. \tag{10.3}$$

The associated flow field $\boldsymbol{u}$ is governed by the linear and homogeneous Stokes equations, and is generated solely by the Marangoni-like term in the shear condition (8.6). It then follows that both this field and the bubble velocity $\mathscr{U}$ must be $O(\lambda)$ as well.

With an asymptotically large velocity, the dominance of advection in the advection–diffusion equation (8.1) implies that c is constant on each streamline. Anticipating that the streamlines are open, originating at infinity where $c = 0$ (see (8.3)), we then find that c actually vanishes at leading-order, and then, recursively, at all asymptotic orders. It is therefore exponentially small (cf. Schnitzer & Yariv 2012*b*). Of course, the very generation of such strong convection requires a (non-zero) asymptotically large distribution at $r = 1$. This apparent paradox is resolved via the introduction of a boundary layer about $r = 1$, allowing the $O(\lambda)$ large concentration to attenuate. Relation (10.2) is then understood to apply within this diffusive boundary layer

https://doi.org/10.1017/jfm.2014.350 Published online by Cambridge University Press

(lying outside the Debye layer). The thickness of this layer, determined from a balance between advection and diffusion, is $\lambda^{-1/2}$. Given (10.3), it is consistently $\ll 1$.

The scaling $\lambda(\beta)$ is determined from the boundary condition (8.2), relating the radial diffusive flux at $r=1$ to the divergence of tangential Debye-scale fluxes. The left-hand side of (8.2), being $O(\lambda^{3/2})$, clearly dominates the $O(\lambda)$ advection term on the right-hand side; it must therefore be balanced by the two $O(\beta)$ terms. We accordingly find

$$\lambda(\beta) = \beta^{2/3} \tag{10.4}$$

which is consistent with the *a priori* assumption (10.3). The boundary-layer thickness is $\beta^{-1/3}$; salt transport within this layer is accordingly described by the stretched normal coordinate

$$R = \beta^{1/3}(r-1). \tag{10.5}$$

Specifically, the concentration deviation within this layer possesses the asymptotic expansion

$$c = \beta^{2/3} C'(R,\theta) + \cdots . \tag{10.6}$$

No comparable boundary layer develops in the hydrodynamic problem, since it depends only upon the value of c at $r=1$ (i.e. $R=0$). Thus, the asymptotic expansion of the flow field $\boldsymbol{u}$ is

$$\boldsymbol{u} = \beta^{2/3}\boldsymbol{u}'(r,\theta) + \cdots , \tag{10.7}$$

with the corresponding expansions of the velocity components in the r and θ directions,

$$u = \beta^{2/3}u'(r,\theta) + \cdots , \quad v = \beta^{2/3}v'(r,\theta) + \cdots , \tag{10.8a,b}$$

and the bubble velocity

$$\mathscr{U} \sim \beta^{2/3}\mathscr{U}' + \cdots . \tag{10.9}$$

The nonlinear scaling of the velocity with β obtained via the above arguments is corroborated by the numerical results at strong fields, see figure 1.

10.2. *Leading-order flow problem*

To derive a well-posed problem governing $\mathscr{U}'$ we need to consider the flow problem in detail. The leading-order flow $\boldsymbol{u}'$ is governed by the homogeneous Stokes equations

$$\boldsymbol{\nabla}\cdot\boldsymbol{u}' = 0, \quad \boldsymbol{\nabla}p' = \nabla^2\boldsymbol{u}' \tag{10.10a,b}$$

and the far-field condition

$$\boldsymbol{u}' \to -\mathscr{U}'\hat{\boldsymbol{\imath}}. \tag{10.11}$$

In addition, it satisfies two conditions at the effective boundary $r=1$. The first,

$$u' = 0 \quad \text{at } r=1, \tag{10.12}$$

follows from (8.7). The second is obtained from (8.6):

$$\frac{\partial v'}{\partial r} - v' = -4\frac{\sinh^2\dfrac{\zeta}{4}}{\cosh\dfrac{\zeta}{2}}\left.\frac{\partial C'}{\partial\theta}\right|_{R=0} \quad \text{at } r=1, \tag{10.13}$$

where use has been made of (10.6). Condition (10.13) resembles (microscale) boundary conditions in Marangoni-like problems (Levich 1962).

Owing to the appearance of the diffusive-layer concentration C' on the right-hand side of (10.13) the flow problem is coupled to the salt transport within the diffusive layer, which we consider next.

https://doi.org/10.1017/jfm.2014.350 Published online by Cambridge University Press

10.3. *Diffusive-layer salt profile*

The boundary-layer problem governing C' is itself coupled to the flow field via the advection term in (8.1). Since this term depends only upon the velocity distribution at $O(\beta^{-1/3})$ radial distances from $r=1$, it is convenient to employ the corresponding Taylor expansions of the velocity components (10.8) about $r=1$, obtained using (10.12):

$$u=\beta^{2/3}(r-1)\left.\frac{\partial u'}{\partial r}\right|_{r=1}+\cdots, \quad v=\beta^{2/3}\left.v'\right|_{r=1}+\cdots. \tag{10.14a,b}$$

The leading $O(\beta^{4/3})$ balance of (8.1) thus reads

$$\frac{1}{\alpha}\frac{\partial^2 C'}{\partial R^2}=\left.\frac{\partial u'}{\partial r}\right|_{r=1}R\frac{\partial C'}{\partial R}+\left.v'\right|_{r=1}\frac{\partial C'}{\partial \theta}. \tag{10.15}$$

Making use of the leading $O(\beta^{2/3})$ continuity equation

$$\frac{\partial u'}{\partial r}+\frac{1}{\sin\theta}\frac{\partial}{\partial\theta}(v'\sin\theta)=0 \tag{10.16}$$

transforms (10.15) into the form

$$\frac{1}{\alpha}\frac{\partial^2 C'}{\partial R^2}=v'(1,\theta)\frac{\partial C'}{\partial\theta}-\frac{R}{\sin\theta}\frac{\mathrm{d}}{\mathrm{d}\theta}\left[v'(1,\theta)\sin\theta\right]\frac{\partial C'}{\partial R} \tag{10.17}$$

where convection shows up only through the 'surface' distribution $v'(1,\theta)$.

The problem governing C' thus consists of the advection–diffusion equation (10.17), the $O(\beta)$ balance of (8.2)

$$\frac{\partial C'}{\partial R}=\left\{6(1+2\alpha)\sinh\frac{\zeta}{2}-6\alpha\zeta\cosh\frac{\zeta}{2}\right\}\cos\theta \quad \text{at } R=0, \tag{10.18}$$

and the large-R decay,

$$C'\to 0 \quad \text{as } R\to\infty, \tag{10.19}$$

representing asymptotic matching with the exponentially-small excess-salt concentration in the outer domain.

The parabolic problem (10.17)–(10.19) is similar to the one solved in the context of strong-field electrophoresis of a solid particle (Schnitzer & Yariv 2012*b*) and the phoretic motion of a highly-conducting drop (Schnitzer *et al.* 2013); the solution is derived in appendix A. For $\zeta>0$ we find

$$C'=-\frac{6(1+2\alpha)\sinh\frac{\zeta}{2}-6\alpha\zeta\cosh\frac{\zeta}{2}}{\sqrt{\alpha\pi}} \times\int_0^\theta\frac{\sin t\cos t}{\sqrt{\xi(\theta)-\xi(t)}}\exp\left\{-\frac{\frac{1}{4}\alpha R^2 v'^2(1,\theta)\sin^2\theta}{\xi(\theta)-\xi(t)}\right\}\mathrm{d}t, \tag{10.20}$$

https://doi.org/10.1017/jfm.2014.350 Published online by Cambridge University Press

where $\xi(\theta)$ is defined by (A 8). (The case of a negatively-charged bubble is readily deduced by symmetry arguments.)

It is anticipated that the above diffusive-layer solution breaks down as $\theta \to \pi$, where the tangential velocity v' approaches zero and the assumptions underlying the diffusion–advection balance are violated. This breakdown is expected to result in the formation of a salt wake emanating from the rear stagnation point. Within this wake, the $O(\delta\beta^{2/3})$ salt advected along the layer to that point is transported downstream.

10.4. *Universal flow problem*

Remarkably, the foregoing analysis results in a self-contained flow problem. Indeed, evaluation of (10.20) at $R = 0$ and substitution into (10.13) furnishes the macroscale shear-stress condition

$$\frac{\partial v'}{\partial r} - v' = L(\zeta, \alpha)\frac{\mathrm{d}}{\mathrm{d}\theta}\int_0^\theta \frac{\sin t \cos t}{\sqrt{\displaystyle\int_t^\theta v'(1,\tau)\sin^2\tau\,\mathrm{d}\tau}}\,\mathrm{d}t \quad \text{at } r = 1 \tag{10.21}$$

where

$$L(\zeta, \alpha) = \frac{24\left\{(1+2\alpha)\sinh\dfrac{\zeta}{2} - \alpha\zeta\cosh\dfrac{\zeta}{2}\right\}\sinh^2\dfrac{\zeta}{4}}{\sqrt{\alpha\pi}\cosh\dfrac{\zeta}{2}}. \tag{10.22}$$

Condition (10.21) suggests the fluid-velocity re-scaling

$$u'(r,\theta) = L^{2/3}\tilde{u}(r,\theta), \quad v'(r,\theta) = L^{2/3}\tilde{v}(r,\theta) \tag{10.23a,b}$$

with a similar definition for $\tilde{p}$; we accordingly define $\mathscr{U}' = L^{2/3}\tilde{\mathscr{U}}$. The velocity field $\tilde{\boldsymbol{u}} = \hat{\boldsymbol{e}}_r\tilde{u} + \hat{\boldsymbol{e}}_\theta\tilde{v}$ is thus governed by a nonlinear problem which is universal in the sense of being independent of any parameters; it consists of the Stokes equations

$$\boldsymbol{\nabla}\cdot\tilde{\boldsymbol{u}} = 0, \quad \boldsymbol{\nabla}\tilde{p} = \nabla^2\tilde{\boldsymbol{u}}, \tag{10.24a,b}$$

the impermeability condition

$$\tilde{u} = 0 \quad \text{at } r = 1, \tag{10.25}$$

the 'shear-stress' condition,

$$\frac{\partial\tilde{v}}{\partial r} - \tilde{v} = \frac{\mathrm{d}}{\mathrm{d}\theta}\int_0^\theta \frac{\sin t\cos t}{\sqrt{\displaystyle\int_t^\theta \tilde{v}(1,\tau)\sin^2\tau\,\mathrm{d}\tau}}\,\mathrm{d}t \quad \text{at } r = 1, \tag{10.26}$$

the far-field approach to a uniform flow

$$\tilde{\boldsymbol{u}} \to -\tilde{\mathscr{U}}\hat{\boldsymbol{\imath}} \quad \text{as } r \to \infty \tag{10.27}$$

and the force-free condition

$$\oint_{r=1}\mathrm{d}A\,\hat{\boldsymbol{e}}_r\cdot\left\{-\tilde{p}\boldsymbol{I} + \boldsymbol{\nabla}\tilde{\boldsymbol{u}} + (\boldsymbol{\nabla}\tilde{\boldsymbol{u}})^\dagger\right\} = \boldsymbol{0}. \tag{10.28}$$

https://doi.org/10.1017/jfm.2014.350 Published online by Cambridge University Press

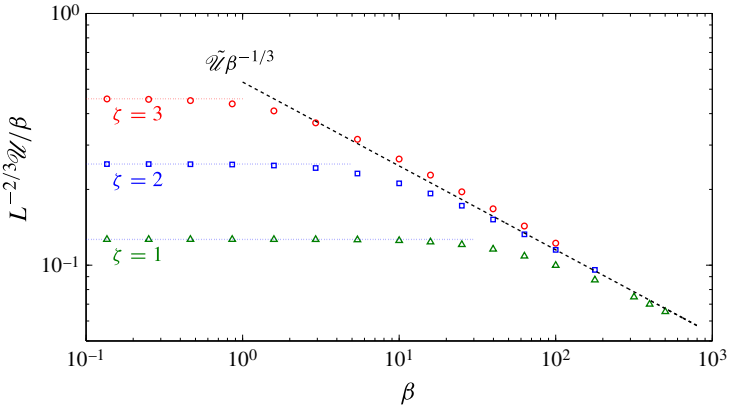


FIGURE 2. (Colour online) Variation of the rescaled electrophoretic mobility with β, the dimensionless field intensity. Presented are the results of the numerical solution of (8.1)–(8.9) for $\alpha = 0.2$ and the indicated values of ζ together with the weak-field approximation (9.19) (dotted lines) and the universal strong-field asymptote (10.29) and (10.30) (dashed line).

We conclude from the above that at large β

$$\mathscr{U} = \tilde{\mathscr{U}}\,\{L(\zeta,\alpha)\beta\}^{2/3}\,, \tag{10.29}$$

providing the scaling with β and the explicit functional dependence upon ζ and α. The value of the pre-factor appearing in (10.29),

$$\tilde{\mathscr{U}} \approx 0.534, \tag{10.30}$$

is obtained by solving the (parameter-free) nonlinear eigenvalue problem (10.24)–(10.28). The details of the solution appear in appendix B.

10.5. *Collapse of the numerical data on the strong-field asymptote*

The strong-field asymptote (10.29) and (10.30) may be compared with our numerical solution of the macroscale problem (8.1)–(8.9). To this end, the numerical results already presented in figure 1 are now recast in figure 2 describing the variation with β of the electrophoretic 'mobility' $\mathscr{U}/\beta$ rescaled by $L^{2/3}$. At relatively small β the respective constant mobility values agree with the corresponding weak-field approximations (9.19). For sufficiently large values of β all the numerical results collapse on the dashed line corresponding to the universal strong-field asymptote (10.29) and (10.30). With decreasing values of ζ, convergence of the numerical results to the strong-field asymptote is deferred to larger values of β, which agrees with the linear velocity dependence upon β in the limit of small ζ, see (9.7).

The agreement of the numerical solution at large β with the asymptote (10.29) and (10.30) *a posteriori* shows that the salt wake inherent in the strong-field limit does not affect the leading-order bubble velocity.

11. Concluding remarks

11.1. *Summary of results*

We have studied bubble electrophoresis in the thin-double-layer limit. To this end, a macroscale model governing transport in the electroneutral bulk has been derived. The

https://doi.org/10.1017/jfm.2014.350 Published online by Cambridge University Press

essence of this model is effective boundary conditions representing the Debye-layer physics and its interaction with the bulk. This description is limited to neither weak fields nor small zeta potentials.

A unique feature of the problem is that the interaction between the applied field and the resulting flow is indirect. Rather, it is here mediated by the salt-concentration perturbation originating from an effective surface-conduction mechanism. The electrophoretic velocity is determined by the coupling between this perturbation and the flow field. Thus, the flow is animated by an effective interfacial shear stress which is linear in the surface gradient of the salt perturbation; this perturbation, in turn, is convected by the flow, affecting both the surface-conduction mechanism and bulk transport. The latter renders the model nonlinear.

Another non-standard feature is the inapplicability of the intuitive linkage between phoretic motion and electro-osmotic slip distribution. As the gas-phase viscosity is negligible compared with that of the suspending liquid, the flow within the latter is decoupled from the internal circulation within the bubble. This results in the absence from the macroscale model of an explicit slip condition, in marked contrast with familiar phoretic models of solid particles. Electro-osmotic slip does in fact relate the macroscale velocities at the liquid and gas phases, but in agreement with the above it merely serves as a boundary condition for the gas flow once the liquid motion has been determined. In fact, as the macroscale model reveals, the liquid flow is driven by an effective shear stress, which may be interpreted as the consequence of an effective non-uniform surface tension. This stress represents Debye-scale osmotic-pressure gradients.

In principle, solving the nonlinear macroscale model provides the bubble velocity as a function of the applied-field magnitude, the zeta potential, and the ion-drag coefficient. We have obtained analytic approximations corresponding to small values of these parameters. In these approximations, the bubble velocity is linear in the applied field. Of particular interest is the case of small zeta potentials, where, in dimensional notation (cf. (9.7)),

$$\mathscr{U}^* = \frac{\epsilon^* \zeta^{*3}}{8\mu^* \varphi^{*2}} E^*. \tag{11.1}$$

As mentioned in the introduction, Booth (1951) obtained an analytic expression for the electrophoretic velocity of drops and bubbles based upon a linearization in small ζ^*. His result is supported by the weak-field numerical computations of Baygents & Saville (1991). In the case of a bubble, Booth's expression yields a zero velocity in the small-δ limit. Expression (11.1) rationalizes this apparent paradox: with a bubble velocity that scales as ζ^{*3}, a linearization in the zeta potential obviously yields a nil value. We note that the small-zeta-potential analysis of Harper (2010) predicts a bubble velocity which is linear in the zeta potential. This is incompatible with both Booth (1951) and the present (11.1). The assumptions underlying Harper's analysis are admittedly not entirely clear to us; we are therefore unable to pinpoint the source of this incompatibility.

For arbitrary values of the governing parameters, the nonlinearity of the macroscale model generally implies a non-constant electrophoretic mobility. Its variation with the applied field has been calculated using numerical simulations; these are straightforward in view of the absence from the macroscale model of the scale disparity associated with the Debye layer. The simulations show a transition from linear electrophoresis at weak fields to a power law at strong fields. The latter limit is of clear practical interest

https://doi.org/10.1017/jfm.2014.350 Published online by Cambridge University Press

for large (e.g. millimetric) bubbles, see (2.19). Within the macroscale framework, the limit of strong fields is singular, where salt polarization is confined to a narrow boundary layer. Detailed asymptotic analysis reveals that the bubble velocity scales as the 2/3-power of the applied-field magnitude and provides the explicit form of the proportionality coefficient. In dimensional notation we find (cf. (10.29))

$$\mathscr{U}^* = \tilde{\mathscr{U}}\,\{L(\zeta,\alpha)\}^{2/3}\,\frac{\epsilon^*\varphi^{*4/3}}{\mu^* a^{*1/3}}E^{*2/3}, \tag{11.2}$$

where $\tilde{\mathscr{U}} \approx 0.534$ and $L(\zeta,\alpha)$ is defined in (10.22).

11.2. *Comparison with Kelsall's experiments*

In the context of electrophoresis of solid particles a general agreement is found between theoretical predictions and experimental observations regarding the (typically linear) scaling of the electrophoretic velocity with the external field. Such is not the case for the electrophoresis of clean bubbles (with mobile surfaces) at the focus of the analyses of Booth (1951) and Harper (2010), as well as that of the present model.

The removal of surfactants was ensured and carefully monitored in the experiments of Kelsall *et al.* (1996*a*,*b*). In these the differences between the rise velocity of gas bubbles in the presence or absence of an external field acting in the direction of gravity were measured. The reported differences scale quadratically with the external field and are thus incompatible with the linear scaling predicted by both Booth (1951) and Harper (2010). (Harper 2010, nevertheless attempts to estimate the bubble charge in the experiments of Kelsall *et al.* through a pointwise fitting procedure which seems of a rather questionable validity.) Evidently, our results predicting the velocity scaling linearly with E^* under weak fields and as $E^{*2/3}$ under strong fields are also at odds with the above-mentioned quadratic scaling.

11.3. *Future directions*

Towards resolving the discrepancy between theory and experimental observations, three possible extensions of the model come to mind.

The first has to do with incorporation of gravity into the model. As already mentioned, Kelsall *et al.*'s experiments (as well as earlier experiments by Brandon *et al.* 1985) focus upon modification of buoyancy effects by the application of external electric fields. In contrast, our theory neglects gravity effects from the outset. Owing to the inherent nonlinearity of the present model, the effect of gravity obviously cannot be incorporated into our analysis via superposition. Rather, this requires an appropriate re-statement of the microscale problem.

The second extension has to do with the underlying physicochemical model of the interface. Our assumption of a uniform surface-charge density, as in Booth (1951), applies to the situation where the concentration of the potential-determining ions (Leroy *et al.* 2012) is sufficiently small compared with that of the salt ions. If this is not the case, one needs to incorporate into the interfacial physicochemical model realistic adsorption kinetics together with an appropriate description of surface-charge transport (Baygents & Saville 1991).

The third extension, which is more subtle, is associated with the limit process appropriate to the description of a gas bubble. In view of the small values of shear viscosity and dielectric permittivity of gases relative to those pertaining to polar

https://doi.org/10.1017/jfm.2014.350 Published online by Cambridge University Press

liquids, we have neglected from the outset the gas-phase contribution to the relevant microscale boundary conditions, namely the mechanical shear-stress balance and the electrostatic Gauss law. While the neglect of the gas-phase contribution to the former does not raise any concerns, one must be cautious when neglecting the gas electric displacement. Indeed, when applying Gauss's law to a slab-shaped control volume spanning the entire double layer (including the charged bubble surface), incorporation of that displacement reveals a field-induced net double-layer charge. It has been pointed out by Baygents & Saville (1989) that the action of the applied field on such charges gives rise to an electrohydrodynamic flow (Melcher & Taylor 1969). In the present context, this effect scales as the product of the gas permittivity and the square of the applied-field magnitude. Thus, despite the smallness of the gas permittivity, under sufficiently strong fields this flow would become comparable to that described in the present analysis, where the velocity approximation (11.2) scales only as the 2/3-power of the applied field.

Acknowledgements

This research was supported by the New York Metropolitan Research Fund and the Israel Science Foundation (grant no. 184/12).

Appendix A. Concentration distribution in the diffusive layer

We employ the coordinate transformation $(R, \theta) \to (\eta, \theta)$, wherein

$$\eta = \sqrt{\alpha} R v'(1, \theta) \sin\theta \tag{A 1}$$

is proportional to the local stream function. The concentration $C'(R, \theta) = \Theta(\eta, \theta)$ is readily found to satisfy the diffusion-type equation

$$\frac{\partial \Theta}{\partial \theta} = v'(1, \theta) \sin^2\theta \frac{\partial^2 \Theta}{\partial \eta^2}, \tag{A 2}$$

the Neumann condition

$$\frac{\partial \Theta}{\partial \eta} = \frac{6(1+2\alpha)\sinh\frac{\zeta}{2} - 6\alpha\zeta\cosh\frac{\zeta}{2}}{\sqrt{\alpha} v'(1, \theta)} \cot\theta \quad \text{at } \eta = 0, \tag{A 3}$$

and the attenuation requirement

$$\Theta \to 0 \quad \text{as } \eta \to \infty. \tag{A 4}$$

For convenience, we analyse the case of a positively-charged bubble ($\sigma > 0$) where, by (4.18), ζ is positive as well. We define the Fourier cosine transform of Θ,

$$\hat{\Theta}(k, \theta) = \sqrt{\frac{2}{\pi}} \int_0^\infty \Theta(\eta, \theta) \cos k\eta \, \mathrm{d}\eta. \tag{A 5}$$

Applying (A 5) to (A 2)–(A 4) yields the first-order differential equation

$$\frac{\partial \hat{\Theta}}{\partial \theta} + k^2 \hat{\Theta}\, v'(1, \theta) \sin^2\theta = -\sqrt{\frac{2}{\alpha\pi}} \left\{ 6(1+2\alpha)\sinh\frac{\zeta}{2} - 6\alpha\zeta\cosh\frac{\zeta}{2} \right\} \sin\theta\cos\theta \tag{A 6}$$

https://doi.org/10.1017/jfm.2014.350 Published online by Cambridge University Press

whose solution is

$$\hat{\Theta} = A(k)\mathrm{e}^{-k^2\xi(\theta)} - \sqrt{\frac{2}{\alpha\pi}}\left\{6(1+2\alpha)\sinh\frac{\zeta}{2} - 6\alpha\zeta\cosh\frac{\zeta}{2}\right\}\int_0^\theta \mathrm{e}^{k^2[\xi(t)-\xi(\theta)]}\sin t\cos t\,\mathrm{d}t, \tag{A 7}$$

in which ξ is given by

$$\xi(\theta) = \int_{\pi/2}^{\theta} v'(1,t)\sin^2 t\,\mathrm{d}t. \tag{A 8}$$

Since a positively-charged bubble is expected to drift in the field direction ($\mathscr{U} > 0$) it is plausible (see (8.8)) that

$$v'(1,\theta) > 0 \quad \text{for } 0 < \theta < \pi, \tag{A 9}$$

implying that $\xi(\theta)$ is a monotonically increasing function for $0 < \theta < \pi$. Thus, the second term in (A 7) decays for large k. On the other hand, since $\xi(\theta) < 0$ for $0 < \theta < \pi/2$, the exponent in the first term of (A 7) diverges in that limit for this range of θ. We therefore find that $A = 0$. Employing the inverse transform and reverting to the original variables then yields (10.20).

Appendix B. Solution of the universal strong-field flow field

The parameter-free flow problem (10.24)–(10.28) governing the pure number $\tilde{\mathscr{U}}$ is solved as follows. We employ the stream function ψ, defined through the relations

$$\tilde{u} = \frac{1}{r^2\sin\theta}\frac{\partial\psi}{\partial\theta}, \quad \tilde{v} = -\frac{1}{r\sin\theta}\frac{\partial\psi}{\partial r}. \tag{B 1a,b}$$

The series expansion (Happel & Brenner 1965)

$$\psi = \tilde{\mathscr{U}}\left(\frac{1}{r} - r^2\right)\mathscr{J}_2(\cos\theta) + \sum_{n=3}^{\infty} k_n\left(r^{1-n} - r^{3-n}\right)\mathscr{J}_n(\cos\theta) \tag{B 2}$$

satisfies the homogeneous Stokes equations (10.24), the impermeability condition (10.25), the force-free constraint (10.28), and the far-field condition (10.27). For convenience we denote $k_2 = \tilde{\mathscr{U}}$. The Gegenbauer polynomials $\mathscr{J}_n$ appearing in (B 2) are related to Legendre polynomials through

$$\mathscr{J}_n(x) = \frac{P_{n-2}(x) - P_n(x)}{2n-1}, \quad n = 2, 3, \ldots, \tag{B 3}$$

with $\mathscr{J}_0(x) = 1$ and $\mathscr{J}_1(x) = -x$. It remains to satisfy the highly nonlinear shear condition (10.26), which, upon substituting (B 2), becomes

$$2\sum_{n=2}^{\infty} k_n(2n-1)\mathscr{J}_n(\mu) = (1-\mu^2)\frac{\mathrm{d}}{\mathrm{d}\mu}\int_\mu^1 \frac{\xi\,\mathrm{d}\xi}{\sqrt{\int_\mu^\xi \tilde{v}(\eta)\sqrt{1-\eta^2}\,\mathrm{d}\eta}}, \tag{B 4}$$

where $\mu = \cos\theta$ and $\tilde{v}(\mu) = \tilde{v}(1,\theta)$. We next multiply (B 4) by $\mathscr{J}_m(\mu)/\sqrt{1-\mu^2}$ and integrate with respect to μ from -1 to 1. Employing the orthogonality relations of the

https://doi.org/10.1017/jfm.2014.350 Published online by Cambridge University Press

Gegenbauer polynomials (Happel & Brenner 1965) and utilizing integration by parts we find

$$k_n = \frac{n(n-1)}{4}\int_{-1}^{1} P_{n-1}(\mu)\int_{\mu}^{1}\frac{\xi\,\mathrm{d}\xi}{\sqrt{\displaystyle\int_{\mu}^{\xi}\tilde{v}(\eta)\sqrt{1-\eta^2}\,\mathrm{d}\eta}}\,\mathrm{d}\mu, \quad n=2,3,\ldots. \tag{B 5}$$

Noting that the antiderivative of $\mathscr{J}_n$ is $(\mathscr{J}_{n+1}-\mathscr{J}_{n-1})/(2n-1)$, and substituting (B 1) and (B 2), we obtain

$$\int_{\mu}^{\xi}\tilde{v}(\eta)\sqrt{1-\eta^2}\,\mathrm{d}\eta = \sum_{m=2}^{\infty} k_m[f_m(\xi)-f_m(\mu)] \tag{B 6}$$

where

$$f_m(t) = \left(\frac{2}{2n-1}+\frac{1}{3}\delta_{m2}\right)\left[\mathscr{J}_{m+1}(t)-\mathscr{J}_{m-1}(t)\right]. \tag{B 7}$$

Thus, we arrive at an algebraic system of nonlinear equations governing the coefficients $\{k_2, k_3, \ldots\}$:

$$k_n = \frac{n(n-1)}{4}\int_{-1}^{1} P_{n-1}(\mu)\int_{\mu}^{1}\frac{\xi\,\mathrm{d}\xi}{\sqrt{\displaystyle\sum_{m=2}^{\infty} k_m[f_m(\xi)-f_m(\mu)]}}\,\mathrm{d}\mu, \quad n=2,3,\ldots. \tag{B 8}$$

This system is solved by controlled truncation and iterations. Our interest mainly lies in the universal bubble velocity, $\tilde{\mathscr{U}} = k_2$, for which the computations yield the value (10.30).

REFERENCES

Batchelor, G. K. 1967 *An Introduction to Fluid Dynamics*. Cambridge University Press.

Baygents, J. C. & Saville, D. A. 1989 The circulation produced in a drop by an electric field: a high field strength electrokinetic model. In *Drops & Bubbles, Third International Colloquium, Monterey 1988* (ed. T. Wang), AIP Conference Proceedings, vol. 7, pp. 7–17. Am. Inst. Phys..

Baygents, J. C. & Saville, D. A. 1991 Electrophoresis of drops and bubbles. *J. Chem. Soc. Faraday Trans.* **87** (12), 1883–1898.

Booth, F. 1951 The cataphoresis of spherical fluid droplets in electrolytes. *J. Chem. Phys.* **19**, 1331–1336.

Brandon, N. P., Kelsall, G. H., Levine, S. & Smith, A. L. 1985 Interfacial electrical properties of electrogenerated bubbles. *J. Appl. Electrochem.* **15** (4), 485–493.

Chang, H.-C. & Yeo, L. Y. 2010 *Electrokinetically Driven Microfluidics and Nanofluidics*. Cambridge University Press.

Choi, K., Kim, S. J., Jin, Y. G., Jang, Y. O., Kim, J.-S. & Chung, D. S. 2008 Single drop microextraction using commercial capillary electrophoresis instruments. *Anal. Chem.* **81** (1), 225–230.

Davis, J. A., James, R. O. & Leckie, J. O. 1978 Surface ionization and complexation at the oxide/water interface: I. Computation of electrical double layer properties in simple electrolytes. *J. Colloid Interface Sci.* **63** (3), 480–499.

Graciaa, A., Morel, G., Saulner, P., Lachaise, J. & Schechter, R. S. 1995 The ζ-potential of gas bubbles. *J. Colloid Interface Sci.* **172** (1), 131–136.

Happel, J. & Brenner, H. 1965 *Low Reynolds Number Hydrodynamics*. Prentice-Hall.

https://doi.org/10.1017/jfm.2014.350 Published online by Cambridge University Press

HARPER, J. F. 2010 Electrophoresis of surfactant-free bubbles. *J. Colloid Interface Sci.* **350** (1), 361–367.

HINCH, E. J., SHERWOOD, J. D., CHEW, W. C. & SEN, P. N. 1984 Dielectric response of a dilute suspension of spheres with thin double layers in an asymmetric electrolyte. *J. Chem. Soc. Faraday Trans.* 2 **80** (5), 535–551.

HUEBNER, A., SHARMA, S., SRISA-ART, M., HOLLFELDER, F., EDEL, J. B. & DEMELLO, A. J. 2008 Microdroplets: a sea of applications? *Lab on a Chip* **8** (8), 1244–1254.

HUNTER, R. J. 2000 *Foundations of Colloidal Science*. Oxford University Press.

KELSALL, G. H., TANG, S., SMITH, A. L. & YURDAKUL, S. 1996*a* Measurement of rise and electrophoretic velocities of gas bubbles. *J. Chem. Soc. Faraday Trans.* **92**, 3879–3885.

KELSALL, G. H., TANG, S., YURDAKUL, S. & SMITH, A. L. 1996*b* Electrophoretic behaviour of bubbles in aqueous electrolytes. *J. Chem. Soc. Faraday Trans.* **92**, 3887–3893.

KHAIR, A. S. 2013 Diffusiophoresis of colloidal particles in neutral solute gradients at finite Péclet number. *J. Fluid Mech.* **731**, 64–94.

KUMAR, A., ELELE, E., YEKSEL, M., KHUSID, B., QIU, Z. & ACRIVOS, A. 2006 Measurements of the fluid and particle mobilities in strong electric fields. *Phys. Fluids* **18**, 123301.

LEROY, P., JOUGNOT, D., REVIL, A., LASSIN, A. & AZAROUAL, M. 2012 A double layer model of the gas bubble/water interface. *J. Colloid Interface Sci.* **388**, 243–256.

LEVICH, V. G. 1962 *Physicochemical Hydrodynamics*. Prentice-Hall.

LIU, H. & DASGUPTA, P. K. 1997 A falling drop for sample injection in capillary zone electrophoresis. *Analyt. Chem.* **69** (6), 1211–1216.

LYKLEMA, J. 1995 *Fundamentals of Interface and Colloid Science*, vol. II. Academic Press.

MCTAGGART, H. A. 1914 The electrification at liquid–gas surfaces. *Phil. Mag.* **27** (158), 297–314.

MELCHER, J. R. & TAYLOR, G. I. 1969 Electrohydrodynamics: a review of the role of interfacial shear stresses. *Annu. Rev. Fluid Mech.* **1**, 111–146.

MORRISON, F. A. 1970 Electrophoresis of a particle of arbitrary shape. *J. Colloid Interface Sci.* **34**, 210–214.

O'BRIEN, R. W. 1983 The solution of the electrokinetic equations for colloidal particles with thin double layers. *J. Colloid Interface Sci.* **92** (1), 204–216.

O'BRIEN, R. W. & WHITE, L. R. 1978 Electrophoretic mobility of a spherical colloidal particle. *J. Chem. Soc. Faraday Trans.* **74**, 1607–1626.

OHSHIMA, H., HEALY, T. W. & WHITE, L. R. 1984 Electrokinetic phenomena in a dilute suspension of charged mercury drops. *J. Chem. Soc. Faraday Trans.* 2 **80** (12), 1643–1667.

QUINCKE, G. 1861 Ueber die fortfiihrüng Materieller theilchen durch strömende Elektricität. *Ann. Phys. Chem.* **115**, 513–598.

RIVETTE, N. J. & BAYGENTS, J. C. 1996 A note on the electrostatic force and torque acting on an isolated body in an electric field. *Chem. Engng Sci.* **51** (23), 5205–5211.

RUSSEL, W. B., SAVILLE, D. A. & SCHOWALTER, W. R. 1989 *Colloidal Dispersions*. Cambridge University Press.

SAVILLE, D. A. 1977 Electrokinetic effects with small particles. *Annu. Rev. Fluid Mech.* **9**, 321–337.

SCHNITZER, O., FRANKEL, I. & YARIV, E. 2013 Electrokinetic flows about conducting drops. *J. Fluid Mech.* **722**, 394–423.

SCHNITZER, O. & YARIV, E. 2012*a* Macroscale description of electrokinetic flows at large zeta potentials: nonlinear surface conduction. *Phys. Rev.* E **86**, 021503.

SCHNITZER, O. & YARIV, E. 2012*b* Strong-field electrophoresis. *J. Fluid Mech.* **701**, 333–351.

TEH, S. Y., LIN, R., HUNG, L. H. & LEE, A. P. 2008 Droplet microfluidics. *Lab on a Chip* **8** (2), 198–220.

VAN DYKE, M. 1964 *Perturbation Methods in Fluid Mechanics*. Academic.

YANG, C., DABROS, T., LI, D., CZARNECKI, J. & MASLIYAH, J. H. 2001 Measurement of the zeta potential of gas bubbles in aqueous solutions by microelectrophoresis method. *J. Colloid Interface Sci.* **243** (1), 128–135.

YARIV, E. 2006 'Force-free' electrophoresis? *Phys. Fluids* **18**, 031702.

YARIV, E., SCHNITZER, O. & FRANKEL, I. 2011 Streaming-potential phenomena in the thin-Debye-layer limit. Part 1. General theory. *J. Fluid Mech.* **685**, 306–334.

https://doi.org/10.1017/jfm.2014.350 Published online by Cambridge University Press